RSC Advances

PAPER

View Article Online
View Journal | View Issue

Cite this: *RSC Adv.*, 2020, **10**, 6850

Light and magnetism dual-gated photoinduced electron transfer-reversible addition–fragmentation chain transfer (PET-RAFT) polymerization†

Lingjuan Hu,‡[a] Qi Wang,‡[a] Xiaomeng Zhang,[a] Haitao Zhao,[a] Zhe Cui,[a] Peng Fu,[a] Minying Liu,[a] Nan Liu,[b] Shengbao He,[b] Xinchang Pang*[a] and Xiaoguang Qiao*[a]

Received 20th December 2019
Accepted 24th January 2020

DOI: 10.1039/d0ra00401d

rsc.li/rsc-advances

A novel raspberry-like γ-Fe_2O_3@carbon dot (CD) nanocatalyst was prepared and applied for photoinduced electron transfer-reversible addition–fragmentation chain transfer (PET-RAFT) polymerization. The nanocatalyst was found to be an efficient photocatalyst in visible light-regulated PET-RAFT polymerization owing to the oxidative quenching mechanism between the photoexcited γ-Fe_2O_3@CDs and the RAFT agent in the PET process. Notably, polymerization can be reversibly ceased in the absence of light or under an external magnetic field. The superparamagnetic nature and high saturation magnetization value (~30.4 emu g^{-1}) of the nanocatalyst contribute to convenient recycling of the nanocatalyst after polymerization. The PET-RAFT polymerization with the nanocatalyst before and after recycling was investigated, which displayed all the characteristics of controlled/living polymerization systems.

Introduction

In recent years, with the development of "living"/controlled radical polymerization,[1–7] the temporal and spatial sequence regulation of polymers is mediated by external stimuli, such as microwaves,[8] ultrasound,[9] light[10–13] or electric pulses.[14] Among these stimuli, light shows the greatest potential for an ideal system because it is cheap, renewable, facile to manipulate, *etc.* Moreover, the introduction of light as an external stimulus in polymerization not only optimizes the reaction conditions, but also achieves the design, synthesis and precise control of complex systems.[15–19] Photo-induced living radical polymerization have been reported in numerous studies,[20–22] among which the photo-induced electron transfer-reversible addition–fragmentation chain transfer (PET-RAFT) polymerization is recognized to be a versatile technique for the synthesis of tailored polymers and fabrication of advanced materials. This so-called PET-RAFT is mediated by photocatalysts that can transfer electrons from excited states to chain transfer agents (CTAs) to generate radicals with the irradiation of light and initiate polymerization.[23] Visible light,[24] near-infrared light and far-red light-induced[25] RAFT polymerizations at various wavelength bands have gained wide attention.

The previously developed polymerized photocatalysts always require metal complexes, such as *fac*-[$Ir(ppy)_3$],[26] $Ru(bpy)_3Cl_2$,[27] zinc porphyrins,[28,29] and semiconducting nanoparticles.[30] Despite the excellent catalytic properties, trace amounts of these photocatalysts remaining in the polymer matrix may cause decomposition of the final polymer products or lethal contamination.[31,32] Therefore, Boyer *et al.* developed some metal-free catalysts such as Eosin Y and halogenated xanthene dyes to avoid metal contamination.[33] Very recently, carbon dots (CDs) have been reported to be used as efficient metal-free photocatalysts in visible-light-regulated PET-RAFT polymerization.[34] As new nanocarbon materials, CDs are well-known for their low toxicity, low cost, good solvent adaptability and excellent photostability. Although such metal-free PET-RAFT systems may be environment-friendly on the whole, the catalysts remaining in the polymer products still create some problems in the performance of the final products. Therefore, it is quite necessary to develop a simple method to separate and recycle the catalysts in order to avoid the negative effect on the final polymer products and realize the reusability of the catalysts simultaneously.

Boyer *et al.* conjugated Eosin Y to the surface of silica nanoparticles and applied it as a recyclable organic

[a]*Henan Joint International Research Laboratory of Living Polymerizations and Functional Nanomaterials, Henan Key Laboratory of Advanced Nylon Materials and Application, School of Materials Science and Engineering, Zhengzhou University, Zhengzhou, 450001, China. E-mail: Pangxinchang1980@163.com; joexiaoguang@hotmail.com*

[b]*China National Tobacco Quality Supervision and Test Centre, Zhengzhou 450001, China*

† Electronic supplementary information (ESI) available. See DOI: 10.1039/d0ra00401d

‡ These authors contributed equally to this work.

nanocatalyst for photo-induced RAFT polymerization.[35] However, the described recycling process relies on centrifugation, which is strongly dependent on the size of silica particles. Magnetic separation is another common separation technique that has been widely used in a number of fields.[36] Contrary to centrifugation, magnetic separation is simpler and more effective. Magnetic semiconductor nanoparticles ($Zn_{0.64}Fe_{2.36}O_4$) have been reported to be recyclable oxytolerant catalysts for sunlight-photolyzed RAFT photopolymerization.[37] The most direct and convenient way is the combination of a photocatalyst with superparamagnetic nanomaterials, such as γ-Fe_2O_3 and Fe_3O_4.[38,39] For example, it has been reported that magnetic Fe_3O_4 combined with the ZnPTPP nanocomposites can be separated from the polymerization system and recycled by simple magnetic decantation.[40] However, the designed catalyst has low saturation magnetization ($\sim$12.9 emu g^{-1}) because of the decrease in dipolar interactions caused by silica. Therefore, the process of recovering the catalyst must rely on extra centrifugation in addition to magnetic separation. To the best of our knowledge, the combination of superparamagnetic materials and CDs as catalysts in PET-RAFT polymerization has never been reported before.

In this paper, novel raspberry-like γ-Fe_2O_3@CD nanocomposites were fabricated and applied as recoverable efficient photocatalysts for PET-RAFT polymerization. The CDs have less effect on the saturation magnetization value of the γ-Fe_2O_3@CD nanocomposites ($\sim$30.4 emu g^{-1}), indicating the high magnetic responsiveness of the catalysts. The excellent efficiency of the hybrid catalysts in the PET-RAFT process was demonstrated by using different monomers. Notably, the polymerization process can be reversibly ceased in the absence of light or under an external magnetic field. After polymerization, the magnetic separation performance and catalysis recoverability of the raspberry-like γ-Fe_2O_3@CD nanoparticles were also evaluated.

Experimental sections

Materials

Methyl methacrylate (MMA, 99%), methyl acrylate (MA, 99%), *n*-butyl methacrylate (BA, 99%), triethylamine (≥99%), styrene (St, 99%), and anhydrous dimethyl sulfoxide (DMSO) were all purchased from Aladdin. The MMA monomers were purified by passing through a basic alumina column (100–200 mesh, purchased from Aladdin) to remove the inhibitors prior to use. Sodium thiosulfate pentahydrate (99%) and sodium citrate tribasic dehydrate (99%) were purchased from J&K Scientific. Blue LED light strips (λ_{max} = 420 nm, 1 m, 6 W, 2 mW cm^{-2}) were purchased from Rishang Optoelectronics Co., Ltd. for visible light-regulated RAFT polymerizations. 4-Cyanopentanoic acid dithiobenzoate (CPADB) was also purchased from Aladdin. For the preparation of γ-Fe_2O_3 nanoparticles, $FeCl_2$ and $FeCl_3$ precursors, ammonium hydroxide solution (NH_4OH, 28–30 wt%) in water, nitric acid (HNO_3, 1 M) and hydrochloric acid (HCl, 36 wt%) were purchased from Sigma-Aldrich. $NH_3 \cdot H_2O$, HNO_3, acetone, ethanol and ether were purchased from Sinopharm Chemical Reagent Co. Ltd. The chemicals were used without any further purification. Deionized (DI) water was used from the laboratory.

Characterizations

Transmission electron microscopy (TEM) analysis was performed with a Philips CM200 microscope at an accelerating voltage of 200 kV. X-ray diffraction (XRD) analysis was performed with an X'Pert PRO polycrystalline powder X-ray diffractometer from Panalytical. The monochromatic Cu Kα ray diffraction was used with a scanning speed of 0.5° min^{-1} and a diffraction angle range of 20–70°. The magnetization curves of the nanoparticles were characterized by a Quantum Design MPMS-5S superconducting quantum interference device (SQUID) magnetometer. ^{1}H-NMR spectra were recorded using a Bruker spectrometer (300 MHz), and all the samples were analyzed using $CDCl_3$ as the solvent. The molecular weights (M_n) of the polymers were measured by using a Waters gel permeation chromatograph (1515 HPLC pump) with THF as the solvent. THF was used as the eluent at a flow rate of 1.0 ml min^{-1} at 35 °C. The UV-vis absorption spectra of the samples were obtained using a Thermo Scientific EV300 UV-vis spectrophotometer. The Fourier transform infrared (FTIR) spectra of the samples were obtained by using a Bruker Spectrum FTIR system. The photoluminescence spectra of the samples were recorded on a Thermo Scientific Lumina spectrofluorometer.

Experimental procedures

Preparation of γ-Fe_2O_3 magnetic nanoparticles. γ-Fe_2O_3 magnetic nanoparticles were synthesized according to a previously reported method with slight modifications.[41] Four mmol $FeCl_2 \cdot 4H_2O$ and 8 mmol $FeCl_3 \cdot 6H_2O$ were first dissolved in 80 ml deionized water at room temperature. Then, 5 ml ammonium hydroxide solution NH_4OH (28 wt%) was quickly added and mechanically stirred for 30 min. After that, the precipitates were collected with a permanent handheld magnet and washed with water and HNO_3. In order to accomplish oxidation, the collected precipitates were dissolved in water, heated to 80 °C, and then stirred for 30 min to obtain an orange turbid liquid. The supernatant was removed after the collection of precipitates with the assistance of a magnet. Finally, the precipitates were first washed once with an HNO_3 and water mixture, then washed three times with acetone and once with diethyl ether, and the obtained solid was dried and redispersed in water for further use.

Hydrothermal synthesis of γ-Fe_2O_3@CD raspberry-like nanoparticles. S-doped γ-Fe_2O_3@CD nanoparticles were synthesized using a previously reported hydrothermal method with slight modifications.[42] First, 1.79 g γ-Fe_2O_3 was mixed with 25 ml aqueous solutions of 0.1 M sodium citrate and 0.3 M sodium thiosulfate and introduced to a 50 ml Teflon-lined stainless-steel autoclave. After that, the reaction vessel was maintained at 200 °C for 6 hours. The resulting solution was dialyzed to remove the excess precursors. After drying in an oven at 80 °C, the solid products of γ-Fe_2O_3@CDs were obtained finally.

PET-RAFT polymerization. In a typical PET-RAFT polymerization procedure, 9.43 mmol MMA (200 equiv.), 0.047 mmol CPADB (1 equiv.), 0.283 mmol TEA (6 equiv.) and 10 mg γ-Fe_2O_3@CD nanoparticles were first dispersed in 1 ml DMSO and then introduced into a glass vial. The glass vial was covered with an aluminum foil to prevent the light during the freeze–pump–thaw cycles for deoxygenation. The reaction was irradiated by a 420 nm LED light source (6 mW cm^{-2}). The samples were periodically taken for further analysis. To study the magnetic response of the nanocatalysts in the reaction system, a strong external magnet was applied for the magnetic control of polymerization and the recyclability of the nanocatalysts.

Results and discussion

Synthesis and characterization of γ-Fe_2O_3 and γ-Fe_2O_3@CD raspberry-like nanoparticles

As illustrated in Scheme 1a, the synthetic route for the preparation of the γ-Fe_2O_3@CD hybrid nanoparticles (NPs) was designed to be an *in situ* growth process. γ-Fe_2O_3 nanoparticles with a high positive charge (+41.9 mV) were first prepared through co-precipitation and strong oxidation by following a previously reported method.[41] Five distinct diffraction peaks can be seen clearly and no other miscellaneous peaks appear in the XRD pattern of the sample, illustrating the successful synthesis of γ-Fe_2O_3 (Fig. S1†). Considering the strong negative charges, the precursors of CDs (−102.3 mV) were supposed to be adsorbed on the surface of γ-Fe_2O_3 and *in situ* grow to form raspberry-like nanocatalysts.

The TEM images show that the obtained magnetic γ-Fe_2O_3 NPs exhibit approximately spherical morphological characteristics with a uniform size of ~30 nm (Fig. 1a). γ-Fe_2O_3 NPs were then mixed with sodium citrate and sodium thiosulfate solutions in aqueous media. During the hydrothermal reaction process, the precursors (oligomers with rich SO^{3-}, COO^{-}, and OH^{-} groups) of CDs appeared gradually and adsorbed on the surface of the γ-Fe_2O_3 nanoparticles owing to the positive and negative electrostatic effects (Fig. S2†). The precursors grew continually to form tiny nodules (CDs) on the surface of γ-Fe_2O_3, and raspberry-like hybrid nanoparticles were finally obtained (Fig. 1c and d). Compared with pure CDs (Fig. 1b, ~5.3 nm), those on the γ-Fe_2O_3 surface had poor uniformity and regularity, which may be due to the confinement of growth and orientation. Even so, it could be seen that both γ-Fe_2O_3@CD and CD nanoparticles had the same UV absorption (Fig. 2a) and strong wide PL emission wavelengths ranging from 400 nm to 520 nm upon excitation using the wavelength of 360 nm, which was attributed to the homogeneous surface structure and size of S-doped CDs (Fig. 2b).[42] These results illustrate the successful coating of CDs on the surface of the γ-Fe_2O_3 nanoparticles.

PET-RAFT polymerization of MMA

As shown in Fig. 3, the PET-RAFT polymerization of MMA using γ-Fe_2O_3@CDs as a photoredox catalyst exhibits all the features of a controlled/living system. Fig. 3a shows the linear evolution of $\ln([M]_0/[M]_t)$ with the exposure time, and such first-order kinetics suggest a constant and steady concentration of growing radicals during polymerization. The GPC traces of PMMA obtained in the kinetic study showed the monomodal distribution of the molecular weight shifting with the exposure time (Fig. 3b). The evolution of M_n showed a linear increase with the increase in molar conversion and gave narrow molar mass distributions (M_w/M_n < 1.2) throughout the polymer, indicating a good control of the polymerization process (Fig. 3d). Notably, the polymerization process can be easily manipulated by switching the light or adopting a magnetic field. The entire polymerization process is mediated by the rapidly reversible activation and deactivation of the nanocatalyst in "ON/OFF" experiments. Fig. 3c shows good temporal control over the polymerization process. In the absence of light, no polymerization was observed, and the polymerization was reinitiated steadily once the light was switched "ON". The experimental molecular weight linearly increased with monomer conversion; it was substantially consistent with the theoretical

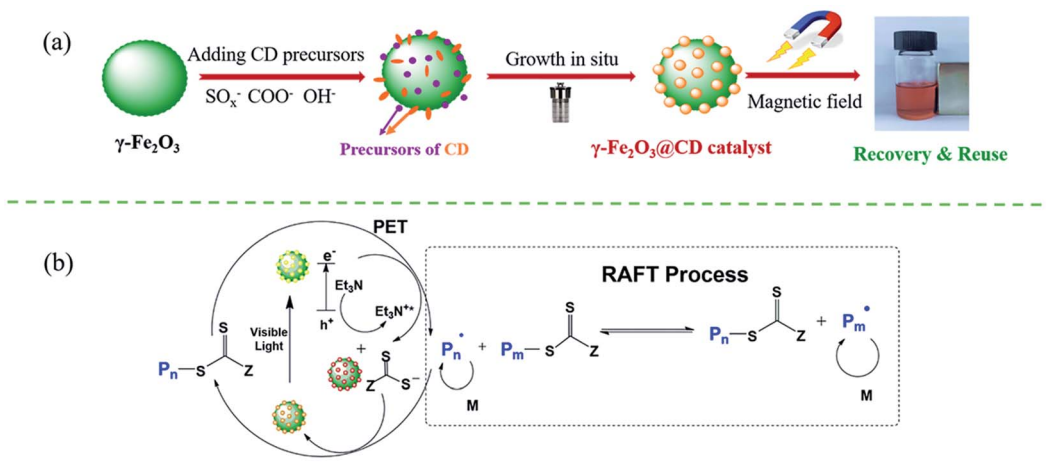

Scheme 1 (a) The design and synthesis of γ-Fe_2O_3@CD nanoparticles *via* the hydrothermal method. (b) Proposed mechanism of γ-Fe_2O_3@CD-catalyzed PET-RAFT polymerization under blue LED light irradiation. The chemical structures of RAFT agents in this study.

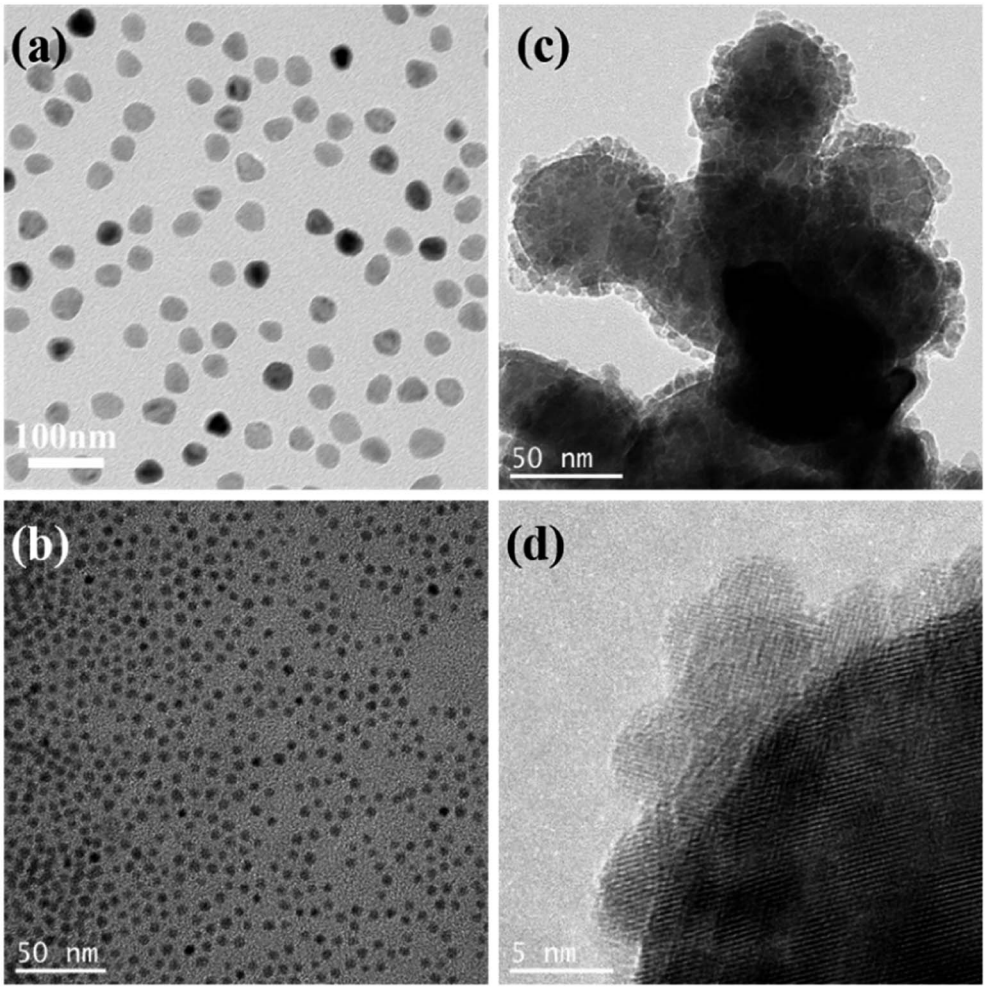

Fig. 1 TEM images of (a) superparamagnetic γ-Fe_2O_3, (b) sulfur-doped carbon dots, (c and d) superparamagnetic γ-Fe_2O_3@CD raspberry-like nanoparticles as the catalysts at different magnifications.

values and showed a narrow dispersity distribution ($M_w/M_n \approx$ 1.19, Fig. 3d). Similarly, the polymerization reaction stopped immediately once the magnetic nanocatalyst was separated from the system due to the highly limited access of CTA to CDs on the surface, which may influence the electron transfer between CDs on the surface of the γ-Fe_2O_3@CD nanocatalyst and the RAFT agent. The polymerization preferentially restarted once the magnetic field was removed (Fig. 3e) as the nanocatalyst could be well re-dispersed in the media according to its superparamagnetic properties. In addition, the living characters of the polymer were

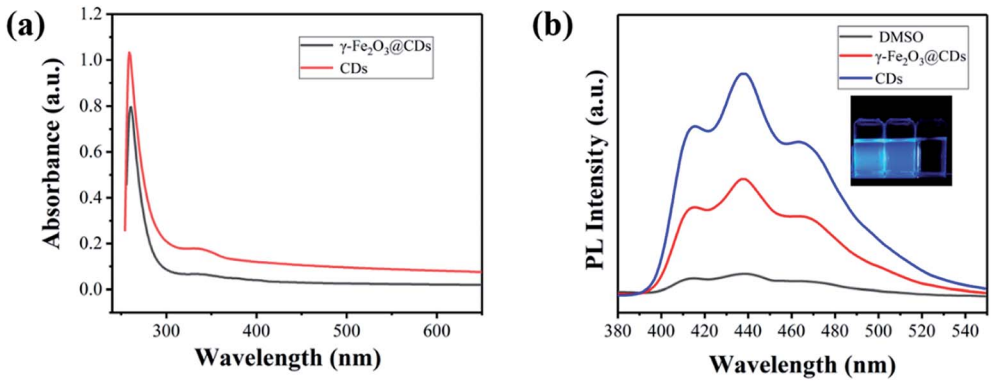

Fig. 2 UV-vis absorption spectrum (a) and photoluminescence spectrum (b) of CDs and superparamagnetic γ-Fe_2O_3@CD nanoparticles dispersed in DMSO (the inset photographs represent CDs, γ-Fe_2O_3@CDs dispersed in DMSO and pure DMSO, respectively).

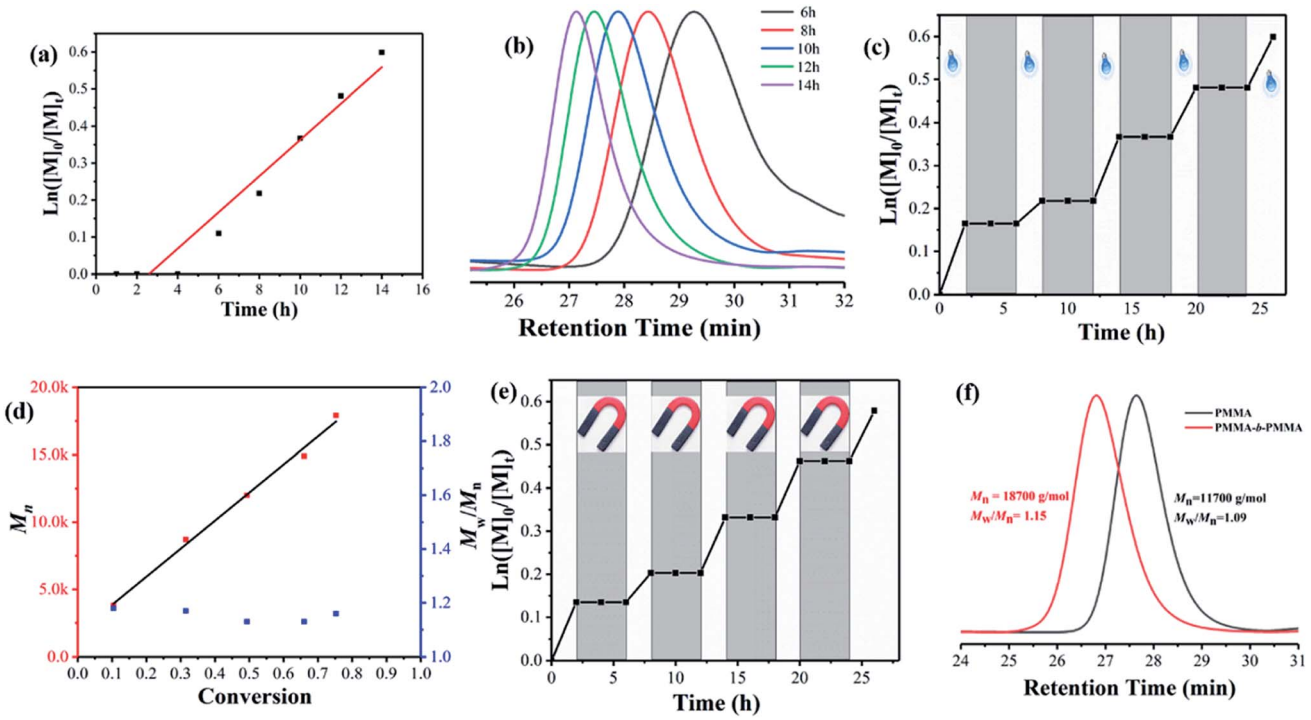

Fig. 3 Kinetic study of PET-RAFT polymerization of MMA catalyzed by γ-Fe_2O_3@CD photocatalyst. (a) Plot of $\ln[M]_0/[M]_t$ *versus* exposure time *t*. (b) GPC traces in the kinetic study of PMMA synthesized *via* PET-RAFT polymerization. (c) Temporal control over polymerization upon switching the light. (d) Number-average molecular weight (M_n) and polydispersity index (PDI) of PMMA synthesized in the kinetic study. (e) Temporal control over polymerization upon adopting a magnetic field; (f) GPC traces of chain extension products for PMMA (black) and PMMA-*b*-PMMA (red).

confirmed through a chain-extension experiment, in which the macro-RAFT agent (PMMA with $M_n = 11\,700$ g mol^{-1}) extended to the polymer chain with $M_n = 18\,700$ g mol^{-1} and a narrow molar mass distribution ($M_w/M_n = 1.15$).

According to the polymerization results, a photoredox quenching mechanism was proposed to explain the effective catalysis of γ-Fe_2O_3@CDs in PET-RAFT polymerization (Scheme 1b). CDs on the surface of γ-Fe_2O_3@CDs were supposed to act as electron acceptors or electron donors *via* electron transfer.[43–45] Photoexcited γ-Fe_2O_3@CDs could undergo charge transfer with the RAFT agent upon light irradiation. The reduced RAFT agent may generate free radicals and oxidize the excited γ-Fe_2O_3@CDs as a degenerative chain transfer agent. The generated free radicals can initiate polymerization and chain growth in

Table 1 Versatility for monomers catalyzed by γ-Fe_2O_3@CD nanoparticles as photocatalysts

Entry[a]	[M] : [CTA]	Monomer	RAFT agent	Time (h)	Conv.[b] (%)	$M_{n,th}$[b] (g mol^{-1})	$M_{n,GPC}$[c] (g mol^{-1})	M_w/M_n
1	200 : 1	MMA	—	24	0	0	0	—
2[d]	200 : 1	MMA	CPADB	48	0	0	0	—
3[e]	200 : 1	MMA	CPADB	24	17.65	3800	4500	1.19
4[f]	200 : 1	MMA	CPADB	24	30.2	6300	7200	1.17
5	200 : 1	MMA	CPADB	24	76.42	15 600	14 200	1.18
6	200 : 1	MA	CPDTC	24	84.43	14 500	20 600	1.12
7	200 : 1	BA	CPDTC	24	48.32	12 700	13 300	1.07
8	200 : 1	St	CDTPA	48	41.29	9000	5100	1.13
9	100 : 1	MMA	CPADB	24	79.33	8200	7700	1.14
10	400 : 1	MMA	CPADB	24	75	30 300	28 900	1.13

[a] The reactions were performed at room temperature with 50% v/v monomer concentration under blue LED light irradiation (6 W, $\lambda_{max} = 460$ nm, 2 mW cm^{-2}) in the absence of oxygen in DMSO ($[M]_0/[CTA] : [TEA] = 200 : 1 : 6$). [b] The molecular weight was calculated using the following equation: $M_{n,NMR} = [M]_0/[CTA] \times M_w^M \times$ conv. $+ M_w^{CTA}$, where $[M]_0$, [CTA], M_w^M, conv. and M_w^{CTA} correspond to initial monomer concentration, initial CTA concentration, molar mass of monomer, monomer conversion determined from ^{1}H NMR spectroscopy, and molar mass of CTA. [c] Molecular weight and polydispersity index were determined by THF GPC analysis calibrated using polystyrene standards. [d] The reaction was carried out in the dark. [e] The reaction was performed without γ-Fe_2O_3@CD nanoparticles. [f] The reaction was performed in the absence of TEA.

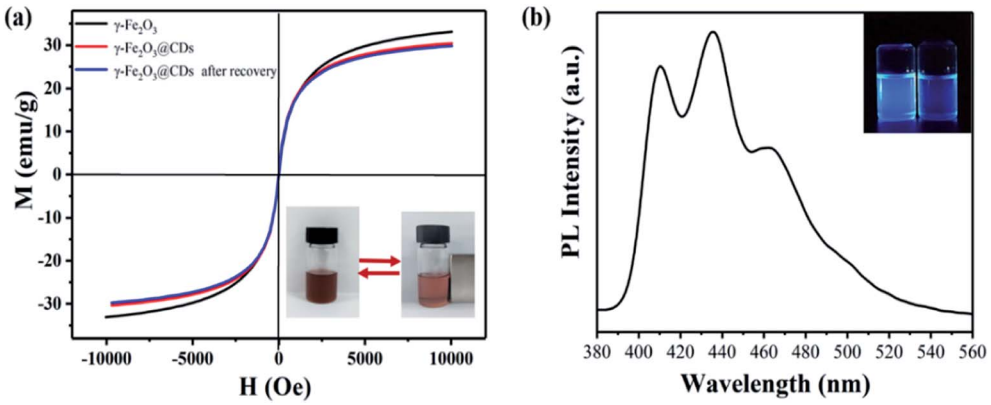

Fig. 4 (a) Field-dependent magnetization of the synthesized γ-Fe_2O_3, γ-Fe_2O_3@CD and γ-Fe_2O_3@CD nanoparticles after recovery. (b) The photoluminescence spectrum of superparamagnetic γ-Fe_2O_3@CD nanoparticles after recovery (the inset picture is a fluorescence photograph of γ-Fe_2O_3@CDs in DMSO and pure DMSO under 360 nm irradiation).

a controlled manner, and the radicals may eventually interact with the oxidized γ-Fe_2O_3@CDs to "reset" the system and complete the catalytic cycle.[46]

In order to demonstrate the electron transfer between γ-Fe_2O_3@CDs and RAFT agents, a fluorescence quenching study was performed (Fig. S5†), showing that the fluorescence emission intensity decreased continuously as the concentration of the RAFT agent increased. In addition, the ratio of I_0/I showed a nonlinear relationship with the concentration of the RAFT agent, demonstrating the electron transfer between the chain transfer agent and γ-Fe_2O_3@CDs. The addition of TEA in the polymerization process may remove the holes as sacrificial electron donors to accelerate the PET-RAFT polymerization rate. Moreover, such PET-RAFT polymerization systems with other types of monomers were investigated, as listed in Table 1. According to the controlled molecular weight and narrow molecular weight distributions ($M_w/M_n < 1.2$) for MA, BA and St, the versatility and universality of the nanocatalysts can be confirmed.

Recovery and reuse of the γ-Fe_2O_3@CD nanocatalyst

Fig. 4a shows the magnetization curves functioned with the magnetic field for pure γ-Fe_2O_3 and γ-Fe_2O_3@CD nanoparticles before and after recovery. The magnetization curves indicate excellent superparamagnetic properties, which are crucial for magnetism-gated PET-RAFT polymerization. As expected, the saturation magnetization value for γ-Fe_2O_3@CDs (~30.4 emu g^{-1}) was smaller than that for pure γ-Fe_2O_3 (~33.1 emu g^{-1}), and this may be due to the shielding effect of the exterior CD shell and the increased interparticle distances between the magnetic γ-Fe_2O_3 nanoparticles. On the other hand, such a small reduction in the saturation magnetization value (2.7 emu g^{-1}) suggested that the CD shell was so thin that the shielding effect was very weak. Moreover, the recycled γ-Fe_2O_3@CD nanoparticles showed almost the same magnetization curves as the one before use, indicating that the CD layer on the surface of γ-Fe_2O_3 (or the raspberry-like hybrid structure) did not change or shield during polymerization and recycling. The γ-Fe_2O_3@CD nanocatalysts could be directly recycled by magnetic separation without centrifugation due to the high magnetic responsiveness (the inset picture in Fig. 4a). Fig. 4b shows that the recycled γ-Fe_2O_3@CD nanoparticles yield bright blue emission when illuminated under UV light (360 nm), indicating that the γ-Fe_2O_3@CD nanoparticles still have excellent fluorescence properties after recovery.

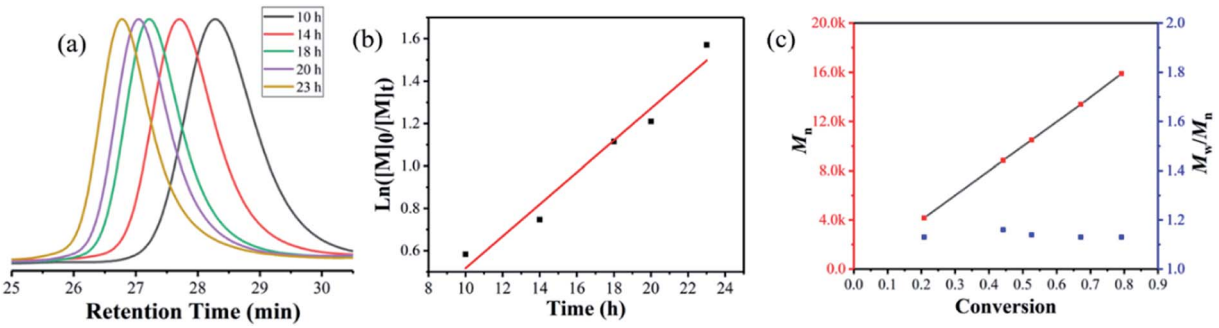

Fig. 5 PET-RAFT polymerization of γ-Fe_2O_3@CD nanoparticles recovered for the second time by magnetic separation at room temperature under blue light irradiation (6 W, $\lambda_{max} = 460$ nm, 2 mW cm^{-2}) in the absence of oxygen at 25 °C in DMSO ($[M]_0/[CTA] = 200:1$). (a) GPC traces in the kinetic study of PMMA synthesized *via* PET-RAFT polymerization for the second time. (b) The relationship between $\ln([M]_0/[M]_t)$ and reaction time; (c) M_n *vs.* monomer conversion and M_w/M_n *versus* conversion.

Table 2 Photocatalytic results of magnetic nanoparticle recycling catalysis of MMA using CDTPA under blue LEDs (λ_{max} = 460 nm, intensity = 2 mW cm^{-2}) as a light source in DMSO[a]

No. of cycles	Time (h)	Conv.[b] (%)	$M_{n,th}$[c] (g mol^{-1})	$M_{n,GPC}$[d] (g mol^{-1})	M_w/M_n
1	24	79.17	16 100	19 000	1.13
2	24	65.32	13 400	16 800	1.23
3	24	62.40	12 800	15 500	1.22
4	24	60.81	12 200	14 800	1.33
5	24	63.52	13 000	14 200	1.17

[a] Reactions were performed in the absence of oxygen at room temperature with 50% v/v monomer concentrations with [MMA] : [CPADB] of 200 : 1. [b] Monomer conversion was determined by using ^{1}H NMR spectroscopy. [c] Theoretical molecular weight was calculated using the following equation: $M_{n,NMR} = [M]_0/[CTA] \times M_w^M \times$ conv. + M_w^{CTA}, where $[M]_0$, [CTA], M_w^M, conv. and M_w^{CTA} correspond to initial monomer concentration, initial CTA concentration, molar mass of monomer, monomer conversion determined from ^{1}H NMR spectroscopy, and molar mass of CTA. [d] Molecular weight and polydispersity index (M_w/M_n) were determined by GPC analysis calibrated to polystyrene standards.

The recycled γ-Fe_2O_3@CD nanoparticles were then applied for PET-RAFT polymerization with MMA. As shown in Fig. 5, very similar polymerization kinetic results are obtained. Although the polymerization rate was slightly slower than that of the polymerization at the first time, the linear evolution of the kinetic plots was observed again. The linear increase in M_n on increasing monomer conversion and the narrow molar mass distribution (M_w/M_n < 1.2) confirmed the excellent control of polymerization. The GPC peaks of the polymer shifted to a higher molar mass with the increase in monomer conversion, which confirmed the living character of the polymerization. These results indicated the excellent catalytic properties and recoverability of the γ-Fe_2O_3@CD nanoparticles in PET-RAFT polymerization.

In order to evaluate the stability of magnetically responsive γ-Fe_2O_3@CD nanoparticles after polymerization and recovery, a series of cycle experiments were performed for at least 5 times, as listed in Table 2. All the monomer conversions exceeded 50 mol% during cyclic polymerization, indicating the high recycling stability of the nanocatalysts (Fig. S9†). However, the conversion of second polymerization was slightly lower than that for the first one, which may be due to the partial aggregation of the γ-Fe_2O_3@CD nanoparticles during the recovery process. The high surface energy of the nanoparticles was suggested to be the reason for aggregation, which resulted in lower catalytic efficiency for polymerization. Relatively narrow molecular weight distributions ($M_w/M_n \leq 1.33$) were observed for all polymerizations, demonstrating good control of the PET-RAFT polymerization with the nanocatalyst.

Conclusions

In summary, recyclable novel dual stimuli-responsive raspberry-like γ-Fe_2O_3@CD photocatalysts have been designed and synthesized through an *in situ* growth process. The precursors of CDs (−102.3 mV) were adsorbed on the surface of γ-Fe_2O_3 (+41.9 mV) based on the positive and negative electrostatic interactions and *in situ* grew to form raspberry-like nanocatalysts. The PET-RAFT polymerization in the presence of the γ-Fe_2O_3@CD nanocatalyst exhibited all the characteristics of controlled radical polymerization with different monomers and displayed magnetic/visible light double regulated behavior. Due to the high magnetization values before (∼30.4 emu g^{-1}) and after recycling (∼30.0 emu g^{-1}), the nanocatalyst could be easily removed by simple magnetic separation from the polymer products and reused repeatedly, making such PET-RAFT processes more sustainable and less-contaminated. Moreover, the raspberry-like nanocatalyst is expected to be applied in various living radical polymerization systems.

Conflicts of interest

There are no conflicts to declare.

Acknowledgements

The work was financially supported by the National Science Foundation of China (Grant No. U1804128, 51973201, to Xinchang Pang), Key R&D and Promotion Special Program of Henan Province (Grant No. 2018-966, to Xinchang Pang), the 111 project (D18023, to Xinchang Pang), the National Science Foundation for Young Scientists of China (Grant No. 51703206, to Zhe Cui), the National Key R&D Program of China (2017YFB0307600, to Minying Liu), the Postdoctoral Research grand in Henan Province (No. 1901007).

Notes and references

1 K. Matyjaszewski, *Macromolecules*, 2012, **45**, 4015–4039.
2 K. Matyjaszewski and N. V. Tsarevsky, *J. Am. Chem. Soc.*, 2014, **136**, 6513–6533.
3 S. Shanmugam, J. Xu and C. Boyer, *Macromol. Rapid Commun.*, 2017, **38**, 1700143.
4 B. Li, Y. Shi and Z. Fu, *J. Polym. Sci., Part A: Polym. Chem.*, 2019, **57**, 1653–1663.
5 H. Sun, L. Yang, M. P. Thompson, S. Schara, W. Cao, W. Choi, Z. Hu, N. Zang, W. Tan and N. C. Gianneschi, *Bioconjugate Chem.*, 2019, **30**, 1889–1904.
6 S. Dadashi-Silab, S. Doran and Y. Yagci, *Chem. Rev.*, 2016, **116**, 10212–10275.
7 X. Pan, M. A. Tasdelen, J. Laun, T. Junkers, Y. Yagci and K. Matyjaszewski, *Prog. Polym. Sci.*, 2016, **62**, 73–125.

8 P. B. Zetterlund and S. b. Perrier, *Macromolecules*, 2011, **44**, 1340–1346.
9 M. Kemmere, M. Kuijpers, L. Jacobs and J. Keurentjes, *Macromol. Symp.*, 2004, **206**, 321–331.
10 J. Phommalysack-Lovan, Y. Chu, C. Boyer and J. Xu, *Chem. Commun.*, 2018, **54**, 6591–6606.
11 P. N. Kurek, A. J. Kloster, K. A. Weaver, R. Manahan, M. L. Allegrezza, N. Boyer, C. De Alwis Watuthanthrige, J. A. Reeves and D. Konkolewicz, *Ind. Eng. Chem. Res.*, 2018, **57**, 4203–4213.
12 A. Wolpers and P. Vana, *Macromolecules*, 2014, **47**, 954–963.
13 Y. Nakamura, T. Arima, S. Tomita and S. Yamago, *J. Am. Chem. Soc.*, 2012, **134**, 5536–5539.
14 C. C. Kathrein, W. K. Kipnusu, F. Kremer and A. Boeker, *Macromolecules*, 2015, **48**, 3354–3359.
15 D. Wei, Y. Xu, C. Liu, Y. Zhai, H. Chen, L. Bai, H. Yang, L. Yang, W. Wang and Y. Niu, *J. Polym. Sci., Part A: Polym. Chem.*, 2019, **57**, 1265–1269.
16 M. Tan, Y. Shi, Z. Fu and W. Yang, *Polym. Chem.*, 2018, **9**, 1082–1094.
17 T. D. Nguyen, S. T. Vo, M. R. Islam, K. T. Lim, D.-V. N. Vo and L. G. Bach, *J. Chem. Technol. Biotechnol.*, 2019, **94**, 1416–1424.
18 Z. Li, H. Tang, A. Feng and S. H. Thang, *Prog. Chem.*, 2018, **30**, 1097–1111.
19 F. A. Leibfarth, K. M. Mattson, B. P. Fors, H. A. Collins and C. J. Hawker, *Angew. Chem., Int. Ed.*, 2013, **52**, 199–210.
20 N. Corrigan, S. Shanmugam, J. Xu and C. Boyer, *Chem. Soc. Rev.*, 2016, **45**, 6165–6212.
21 X. Pan, M. Fantin, F. Yuan and K. Matyjaszewski, *Chem. Soc. Rev.*, 2018, **47**, 5457–5490.
22 A. J. Teator, D. N. Lastovickova and C. W. Bielawski, *Chem. Rev.*, 2015, **116**, 1969–1992.
23 J. Xu, K. Jung, A. Atme, S. Shanmugam and C. Boyer, *J. Am. Chem. Soc.*, 2014, **136**, 5508–5519.
24 Y. Song, Y. Kim, Y. Noh, V. K. Singh, S. K. Behera, A. Abudulimu, K. Chung, R. Wannemacher, J. Gierschner, L. Lüer and M. S. Kwon, *Macromolecules*, 2019, **52**, 5538–5545.
25 S. Shanmugam, J. Xu and C. Boyer, *Angew. Chem., Int. Ed.*, 2016, **55**, 1036–1040.
26 W. Ma, H. Chen, Y. Ma, C. Zhao and W. Yang, *Macromol. Chem. Phys.*, 2014, **215**, 1012–1021.
27 J. Xu, K. Jung and C. Boyer, *Macromolecules*, 2014, **47**, 4217–4229.
28 S. Shanmugam, J. Xu and C. Boyer, *J. Am. Chem. Soc.*, 2015, **137**, 9174–9185.
29 N. Corrigan, D. Rosli, J. W. J. Jones, J. Xu and C. Boyer, *Macromolecules*, 2016, **49**, 6779–6789.
30 Y. Huang, Y. Zhu and E. Egap, *ACS Macro Lett.*, 2018, **7**, 184–189.
31 E. Kolvari, M. Zolfigol, N. Koukabi and B. Shirmardi-Shaghasemi, *Chem. Pap.*, 2011, **65**, 898–902.
32 S. V. Bhagwat, S. Jouen, D. C. Kundaliya, H. Singh, T. Jagadale, A. A. Athawale and S. B. Ogale, *J. Nanosci. Nanotechnol.*, 2009, **9**, 5823–5828.
33 J. Xu, K. Jung, N. A. Corrigan and C. Boyer, *Chem. Sci.*, 2014, **5**, 3568–3575.
34 J. Jiang, G. Ye, Z. Wang, Y. Lu, J. Chen and K. Matyjaszewski, *Angew. Chem., Int. Ed.*, 2018, **57**, 12037–12042.
35 S. Shanmugam, S. Xu, N. N. M. Adnan and C. Boyer, *Macromolecules*, 2018, **51**, 779–790.
36 K. Kołątaj, R. Ambroziak, M. Kędziora, J. Krajczewski and A. Kudelski, *Appl. Surf. Sci.*, 2019, **470**, 970–978.
37 J. Wang, M. Rivero, A. Muñoz Bonilla, J. Sanchez-Marcos, W. Xue, G. Chen, W. Zhang and X. Zhu, *ACS Macro Lett.*, 2016, **5**, 1278–1282.
38 L. Bartolome, M. Imran, K. G. Lee, A. Sangalang, J. K. Ahn and D. H. Kim, *Green Chem.*, 2014, **16**, 279–286.
39 Y. F. Yang, F. Y. Meng, X. H. Li, N. N. Wu, Y. H. Deng, L. Y. Wei and P. Zeng, *J. Nanosci. Nanotechnol.*, 2019, **19**, 7517–7525.
40 X. Li, J. L. Li, W. G. Huang, X. Z. Zhang, B. Zhang and T. Cai, *Nanoscale*, 2018, **10**, 19254–19261.
41 K. Li, P. Y. Dugas, M. Lansalot and E. Bourgeat-Lami, *Macromolecules*, 2016, **49**, 7609–7624.
42 Q. Xu, P. Pu, J. Zhao, C. Dong, C. Gao, Y. Chen, J. Chen, Y. Liu and H. Zhou, *J. Phys. Chem. A*, 2015, **3**, 542–546.
43 Z. Huang, L. Feng, H. Ming, C. Li, T. Xu, C. Chen and X. Guo, *J. Lumin.*, 2014, **151**, 100–105.
44 V. Strauss, J. T. Margraf, K. Dirian, Z. Syrgiannis, M. Prato, C. Wessendorf, A. Hirsch, T. Clark and D. M. Guldi, *Angew. Chem.*, 2015, **127**, 8410–8415.
45 A. Cadranel, V. Strauss, J. T. Margraf, K. A. Winterfeld, C. Vogl, L. Dordevic, F. Arcudi, H. Hoelzel, N. Jux, M. Prato and D. M. Guldi, *J. Am. Chem. Soc.*, 2018, **140**, 904–907.
46 X. Wang, L. Cao, F. Lu, M. J. Meziani, H. Li, G. Qi, B. Zhou, B. A. Harruff, F. Kermarrec and Y. P. Sun, *Chem. Commun.*, 2009, 3774–3776.